APPLIED PHYSICS LETTERS **92**, 212111 (2008)

A-plane GaN epitaxial lateral overgrowth structures: Growth domains, morphological defects, and impurity incorporation directly imaged by cathodoluminescence microscopy

B. Bastek,[1,a)] F. Bertram,[1] J. Christen,[1] T. Wernicke,[2] M. Weyers,[2] and M. Kneissl[2,3]
[1]*Institute of Experimental Physics, Otto-von-Guericke-University Magdeburg, P.O. Box 4120, 39160 Magdeburg, Germany*
[2]*Ferdinand-Braun-Institut für Höchstfrequenztechnik, Gustav-Kirchhof-Staße 4, 12489 Berlin, Germany*
[3]*Institute for Solid State Physics, Technical University Berlin, Berlin, Hardenbergstraße 36, 10623 Berlin, Germany*

(Received 1 April 2008; accepted 17 April 2008; published online 29 May 2008)

The distinctly different growth domains of *a*-plane epitaxial lateral overgrown GaN on stripe masks oriented along $[01\bar{1}0]$ direction were directly visualized by highly spatially and spectrally resolved cathodoluminescence microscopy. Clear cut microscopic regions dominated by differing individual peak wavelengths originating from either basal plane stacking faults, prismatic stacking faults, impurity related donor-acceptor pair or (D^0,X) emission are explicitly correlated to the different growth domains. The luminescence in the domains grown in [0001] direction over the mask [epitaxial lateral overgrown wings] is dominated by the intense and sharp (D^0,X) emission at 3.471 eV. Here, no luminescence originating from morphological defects is found over several micrometers. This evidences the excellent material quality of the *a*-plane GaN, which is fully relaxed at the surface of the wings. © *2008 American Institute of Physics*.
[DOI: 10.1063/1.2920846]

As a consequence of the wurtzite crystal structure group-III nitrides exhibit large spontaneous polarization and -if under strain- piezoelectric fields. Although providing a unique potential for electronic devices,[1] these polarization fields have negative impact on the performance of light emitting devices.[2,3] Resulting from the spatial separation of electrons and holes in quantum well structures with *c*-axis orientation the oscillator strength is reduced and the emission wavelength is redshifted due to the quantum confined Stark effect. Growth in nonpolar crystal orientations eliminates this problem. Epitaxial growth of *a*-plane GaN on *r*-plane sapphire has been reported by several groups.[4–6] However, *a*-plane GaN still suffers from reduced crystalline quality as compared to conventional *c*-plane material, showing higher dislocation densities and considerably more structural defects.[7] In particular basal plane stacking faults (BSFs) are an inherent problem in *a*-plane GaN layers. Usually the BSF luminescence completely dominates the emission spectrum.[8,9] The BSF acts as a polytypic quantum well, yielding a very efficient radiative recombination channel.[10] Several approaches for reducing the dislocation density have been demonstrated for *c*-plane GaN.[11] Remarkable progress has been reported by adapting the technique of epitaxial lateral overgrowth (ELO) to non-*c*-plane growth. ELO of *a*-plane GaN on *r*-plane sapphire substrate has been demonstrated.[12–14] These structures have striped regions of high and low defect densities.[15,16] Quantum structures grown on top of the coalescent layers show a good optical quality and high quantum efficiency.[17–19]

In this paper, we demonstrate that ELO is a suitable method to achieve *a*-plane GaN material of high luminescence quality emitting exclusively near band gap excitonic luminescence. We analyze the local distribution of the different emission channels on a submicrometer scale. The distinctly different characteristic growth domains of *a*-plane ELO-GaN were directly imaged by highly spatially and spectrally resolved cathodoluminescence microscopy (CL).

The noncoalescent *a*-plane ELO samples were grown on *r*-plane sapphire substrate using a 1.8 μm thick GaN template grown by metal organic vapor phase epitaxy (MOVPE). This template was masked with 100 nm thick SiO_2 stripes oriented in $[01\bar{1}0]$ direction (period: 15 μm; opening: 5 μm) and subsequently overgrown using MOVPE (for details see Ref. 20). ELO is stopped before coalescence is reached so that the different growth facets can be studied. Low temperature CL measurements were performed in a home-built setup based on a scanning electron microscope (SEM). In CL imaging mode the focused electron beam is scanned over the selected area (typically 256×200 pixel) and the complete CL spectra are recorded at each pixel resulting in a three-dimensional data set $I_{CL}(x,y,\lambda)$.[21,22]

SEM images of the cross section of an individual *a*-plane oriented GaN stripe cleaved parallel to the *m*-plane are depicted in Figs. 1(a) and 1(c). The resulting ELO-GaN stripes exhibit a width of 8.9 μm and a height of 7.7 μm. The mask openings where the coherent growth in *a* direction took place as well as the +*c*-axis lateral overgrowth regions (to the left) are clearly resolved. The asymmetric lateral overgrowth is clearly visible. While extended lateral overgrowth occurs in [0001] direction almost no ELO is observed in the $[000\bar{1}]$ direction, as reported by Wu *et al.*,[23] Netzel *et al.*,[20] and Wu *et al.*[24]

The two different viewing angles in Fig. 1 allow a direct comparison of the N-face $(000\bar{1})$ side facet [(a) and (b)] as well as the Ga-face (0001) side facet [(c) and (d)] of the ELO stripes. Figure 1(b) depicts the corresponding CL peak wavelength image (CLWI), i.e., a mapping of the local CL peak wavelength, in the spectral range from 350 to 390 nm. Well defined microscopic patterns of different CL peak wavelengths corresponding to the BSFs (363 nm) or the prismatic

a)Electronic mail: barbara.bastek@student.uni-magdeburg.de.

 © 2008 American Institute of Physics
Downloaded 02 Jun 2008 to 62.141.180.1. Redistribution subject to AIP license or copyright; see http://apl.aip.org/apl/copyright.jsp

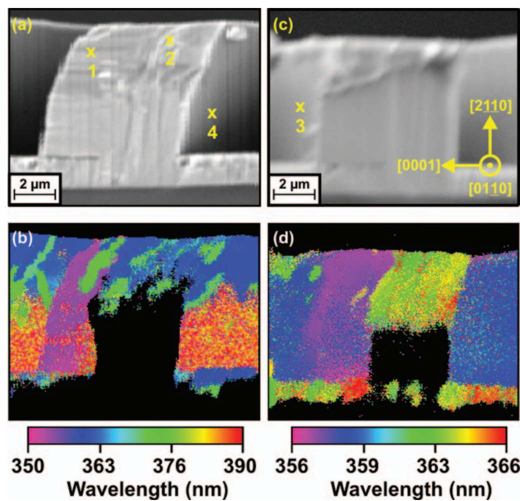

FIG. 1. (Color) [(a) and (c)] SEM images of the sample cross section perpendicular to $[01\bar{1}0]$ under different view angles showing the (0001) facet (a) and the $(000\bar{1})$ facet (c), respectively. [(b) and (d)] lateral mapping of the local CL peak wavelength of the cross sections on top visualizing the individual ELO growth domains. Note the higher spectral resolution in (d) as compared to (b).

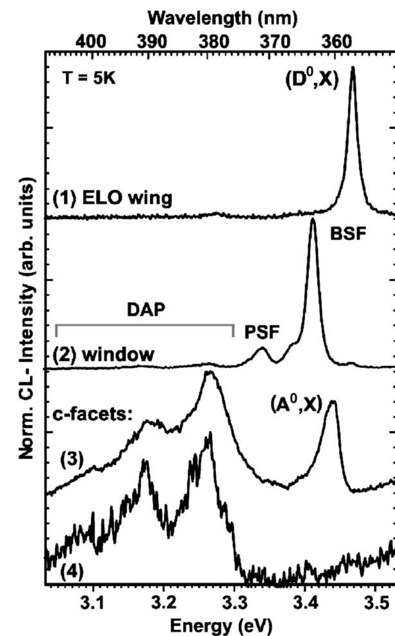

FIG. 2. Local spot CL spectra taken at the positions indicated in Figs. 1(a) and 1(c). (+c) ELO domain (1), upper domain of coherent growth on top of the mask windows (2), lower part of the (−c) side facet (3), and (+c) side facet (4).

stacking faults (PSFs) (371 nm) (Refs. 9 and 25) as well as bound excitons [(D^0,X) at 357 nm and (A^0,X) at 359 nm] and donor-acceptor pair band recombination (DAP) (at 380 nm) are present. These individual emissions channels are clearly locally resolved and allow a direct correlation between the luminescence and the characteristic individual ELO growth domains.

In the first 4–5 μm of coherent a-axis growth directly above the mask openings, almost no luminescence intensity is detected. Hence, this part of the CLWI is masked in black. Here, the material exhibits a high dislocation density causing strong nonradiative recombination and low quantum efficiency. This indicates that the dislocations are efficiently confined in this area of coherent growth. With ongoing growth along $[2\bar{1}\bar{1}0]$ above the mask openings, the quantum efficiency recovers and striations of either dominant BSF (blue contrast, 363 nm) or PSF (green contrast, 371 nm) luminescence become visible.

At the N-face $(000\bar{1})$ facetted sidewall, the DAP band emission at 380 nm dominates for the first 4 μm above the GaN template (red contrast) while for the topmost 4 μm the BSF luminescence is dominating as indicated by the blue contrast. In Fig. 1(d), the CLWI of the sample cross section (c) is shown within the spectral range of the excitonic and BSF luminescence, i.e., for higher spectral resolution. Due to the changed view angle now the Ga-face (0001) side facet is visible. It is clearly obvious that the (A^0,X) (blue contrast, 359 nm) emission is very strong and exclusively detected at this side facet. This spectral asymmetry between $(000\bar{1})$ and (0001) is a direct consequence of the different surface kinetics, resulting in faster growth and less impurity incorporation for the Ga-face facet and a slower growth and enhanced impurity incorporation for the N-face facet.

The laterally overgrown wing region is dominated by the (D^0,X) emission at 357 nm (magenta contrast). Contrary to "normal" a-plane GaN the (D^0,X) luminescence dominates the stacking fault luminescence in this growth domain, evidencing the excellent crystal quality of the GaN in the ELO wing region. A slight vertical blueshift of the spectral position of (D^0,X) of up to 6 meV from the template to the topmost area visualizes vertical relaxation of residual tensile stress on top of the SiO_2 mask. In Fig. 2, spectrum (1) is exactly taken from the a-plane top facet of this overgrown region. Exclusively the intense, sharp (D^0,X) emission at 3.471 eV is visible. No BSF, PSF or other defect-related luminescence is found here.

In complete agreement with the CLWIs, spectrum (2) from the region of coherent a-axis growth above the mask window is dominated by the BSF luminescence at 3.41 eV (363 nm). In addition, we find PSF related luminescence around 3.34 eV (371 nm) and a weak appearance of DAP luminescence at 3.25 eV followed by LO phonon replicas. Only a faint trace of (D^0,X) emission is visible here. These spectral features are typical for normal a-axis grown GaN. The comparison of local spectra (1) and (2) clearly demonstrate the impact of ELO significantly improving the structural quality of a-plane GaN.

Unlike the ELO domains described above, the c facets exhibit no BSF but solely impurity related luminescence and are dominated by the DAP band and its phonon replicas. Again the distinct difference between Ga face and N face is obvious. While spectrum (3) emitted from the (0001) (+c) facet shows intense (A^0,X) luminescence at 3.44 eV (360 nm) in addition to the DAP band, spectrum (4) taken from the lower part of the (0001) (−c) facet solely shows DAP and no excitonic contribution is found. The much lower growth rate of the N-face (0001) facet apparently leads to significantly higher impurity incorporation during ELO.

In order to get deeper insight into the different ELO domains plan view SEM/CL investigation were performed with higher spectral resolution in the near band edge regime. A top view SEM image is depicted in Fig. 3(a). The CLWI of the identical area, shown in Fig. 3(b), exhibits well defined individual stripes running parallel to the mask openings dominated by either BSF, (D^0,X), or (A^0,X) luminescence (note that DAP is outside the spectral range). These individual emissions are clearly locally resolved and perfectly

Downloaded 02 Jun 2008 to 62.141.180.1. Redistribution subject to AIP license or copyright; see http://apl.aip.org/apl/copyright.jsp

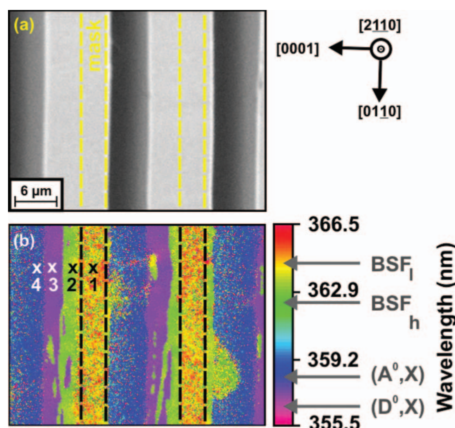

FIG. 3. (Color) (a) SEM image. (b) Lateral mapping of the CL peak wavelength (near band edge CL).

match the four different lateral growth domains:

(a) In the domain of coherent a-axis growth (1) directly above the mask window the broad BSF luminescence dominates the emission (spotty red-yellow contrast).

(b) Continuing in $(+c)$ direction, this region is bounded by a thin stripe (2) where the BSF turns from the spotty contrast to a homogeneous, monochromatic green appearance (363.1 nm). The BSF luminescence becomes sharper and shifts to higher energies. This region marks the boundary between the coherently grown domain and the ELO domain. This transition is even better seen in the local spot mode spectra in Fig. 4 [the spectra are taken at the positions marked in Fig. 3(a)]. While spectrum (1) originating from the coherently grown area (1) directly above the mask openings is dominated by the broad low energetic BSF luminescence at 3.407 eV and no excitonic luminescence is present, spectrum (2) taken at the boundary region shows a narrowing of the BSF luminescence and an increase in its peak energy by 7.2 meV. Hence, clearly two individual components of the BSF luminescence peak can be spectrally and locally discriminated. They can be assigned to individual BSFs of different sizes and shapes.[24]

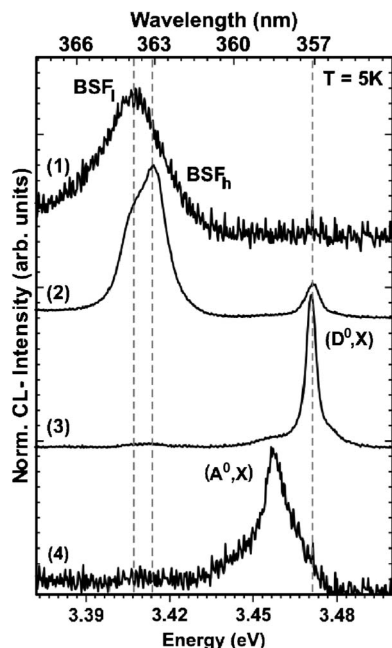

FIG. 4. Highly spectrally resolved local CL spectra taken from the ELO growth domains indicated in Fig. 3(b). (1) domain of coherent a-axis growth on top of the mask openings, (2) boundary region between domain (1) and the ELO domain, (3) domain of $(+c)$-axis lateral overgrowth (ELO wing), and (4) Ga-face side facet (0001).

(c) The ELO wing surface region (3) shows dominant sharp (D^0,X) emission (homogeneous magenta contrast at 357.1 nm). Local spectra taken from the a-plane top surface in the $(+c)$-axis ELO domain (3) exclusively show the intense and sharp (D^0,X) emission at 3.471 eV (full width at half maximum=4.4 meV), corresponding to fully relaxed GaN.[26] No PSF or other defect-related CL is found here. Only some stripes of the BSF luminescence extend into this region. This is attributed to sporadic individual BSFs spontaneously formed in that area as concluded from transmission election microscopy studies published elsewhere.[24]

(d) Finally, the Ga-face (0001) $(+c)$ facet (4) emits exclusively weak (A^0,X) luminescence at 3.457 eV (358.5 nm) visualized by the blue contrast in Fig. 3(b).

In conclusion, we have demonstrated that ELO by MOVPE provides a promising tool for achieving high quality a-plane GaN material. The distinct characteristic individual growth domains have been identified and directly imaged by spectrally resolved CL microscopy. Two individual components of the dominating structural defect BSF were attributed to specific regions in the microstructure. While the a-axis grown GaN on top of the mask windows solely shows the low energy component of BSF, the transition region to lateral growth is dominated by bright BSF luminescence at higher energy. After further lateral growth in $(+c)$ direction a 4 μm wide ELO wing domain of perfect optical quality a-plane GaN evolves, exclusively emitting bright and sharp (D^0,X) luminescence. While slightly redshifted at the wing bottom, the spectral position of (D^0,X) evidences a complete relaxation of residual tensile stress at the ELO wing surface. Asymmetric incorporation of acceptors on the Ga-face and N-face {0001} side facets accompanying the different growth rates was discussed.

[1] O. Ambacher et al., J. Appl. Phys. 85, 3222 (1999).
[2] T. Deguschi et al., Jpn. J. Appl. Phys., Part 2 38, L914 (1999).
[3] P. Lefebvre et al., Phys. Rev. B 59, 15363 (1999).
[4] M. D. Craven et al., Appl. Phys. Lett. 84, 1281 (2004).
[5] A. Chakraborty et al., Appl. Phys. Lett. 89, 041903 (2006).
[6] X. Ni. et al., J. Cryst. Growth 290, 166 (2006).
[7] D. N. Zakharov et al., Phys. Rev. B 71, 235334 (2005).
[8] P. P. Paskov et al., J. Appl. Phys. 98, 093519 (2005).
[9] R. Liu et al., Appl. Phys. Lett. 86, 021908 (2005).
[10] L. Chen et al., "Structural defect-related photoluminescence in GaN," MRS Symposia No. 798 (Materials Research Society, Pittsburgh, 2004), p. Y5.55.1.
[11] J. Christen and T. Riemann, Phys. Status Solidi B 228, 419 (2001).
[12] C. Chen et al., Jpn. J. Appl. Phys., Part 2 42, L818 (2003).
[13] B. A. Haskell et al., Appl. Phys. Lett. 83, 644 (2003).
[14] B. M. Imer et al., Appl. Phys. Lett. 88, 061908 (2006).
[15] P. Vennéguès et al., Jpn. J. Appl. Phys., Part 1 46, 4089 (2007).
[16] T. Guehne et al., J. Appl. Phys. 101, 113101 (2007).
[17] A. Chitnis et al., Appl. Phys. Lett. 84, 3663 (2004).
[18] A. Chakraborty et al., Appl. Phys. Lett. 86, 031901 (2005).
[19] E. Kuokstis et al., Appl. Phys. Lett. 84, 2998 (2004).
[20] C. Netztel et al., J. Cryst. Growth 310, 8 (2008).
[21] J. Christen et al., J. Vac. Sci. Technol. B 9, 2358 (1991).
[22] F. Bertram et al., Appl. Phys. Lett. 74, 359 (1999).
[23] F. Wu et al., J. Appl. Phys. 94, 942 (2003).
[24] Z. H. Wu et al., Appl. Phys. Lett. 92, 171904 (2008).
[25] J. Mei et al., Appl. Phys. Lett. 88, 141912 (2006).
[26] H. Siegle et al., Appl. Phys. Lett. 71, 2490 (1997).

Downloaded 02 Jun 2008 to 62.141.180.1. Redistribution subject to AIP license or copyright; see http://apl.aip.org/apl/copyright.jsp